CONTROL OF EMULSION DROP PRODUCTION

IN FLOW FOCUSING MICROFLUIDICS

A Thesis

by

HAEJUNE KIM

Submitted to the Office of Graduate Studies of
Texas A&M University
in partial fulfillment of the requirements for the degree of

MASTER OF SCIENCE

August 2007

Major Subject: Mechanical Engineering

CONTROL OF EMULSION DROP PRODUCTION

IN FLOW FOCUSING MICROFLUIDICS

A Thesis

by

HAEJUNE KIM

Submitted to the Office of Graduate Studies of
Texas A&M University
in partial fulfillment of the requirements for the degree of

MASTER OF SCIENCE

Approved by:

Co-Chairs of Committee,	Ali Beskok
	Zhengdong Cheng
Committee Member,	Debjyoti Banerjee
Head of Department,	Dennis O'Neal

August 2007

Major Subject: Mechanical Engineering

ABSTRACT

Control of Emulsion Drop Production

in Flow Focusing Microfluidics.

(August 2007)

Haejune Kim, B.S., Korea University

Co-Chairs of Advisory Committee: Dr. Ali Beskok
Dr. Zhengdong Cheng

Generating droplets using flow-focusing microfluidics in multiphase flows has reached its limit that it cannot generate submicrometer droplets in size. Flow focusing geometry together with an electric field has been used to make smaller droplets in microchannels. The droplet size was controllable by the flow rate ratio as well as the electric field. The droplets size decreased as the voltage increased. A Taylor cone was formed to generate very fine droplets which were less than 1 μm in diameter. The tip made smaller droplets due to the tangential force by the electric field. A small inner flow rate and high electric field were required to form a stable Taylor cone in a DC electric field. The droplet size, however, was not stable at a small water flow rate because the flow rate was not as accuate as required. When I used a modified syringe pump with more accurate flow rate control, I was able to obtain a stable set of data. A small change in droplet size occurred at low voltage. The drop size changed dramatically, when the voltage was high enough. I also observed how an AC electric field affects the droplet size. The droplet size was not solely determined by the voltage. This is because

of the imbalance of the supplied flow rate and the emitted flow rate. I also found that the droplet size is related to the tip position of the dispersed phase. The droplet size decreased as the tip stretched more.

Typically, the microfluidic device generated monodispese droplets in narrow size distribution. It also generated a bigger droplet followed by a smaller one consecutively at low flow rate ratio of inner and outer fluid flow $\left(0.09 \le Q_i / Q_o \le 0.265\right)$. To understand this instability of drop formation, a numerical calculation was conducted. The simulation results showed inside of the tip still pointed downstream after it generated a big droplet. Then, the tip generated another smaller droplet while the tip was stretched. Finally, the tip moved back and began a new cycle.

DEDICATION

This thesis is dedicated to my family and my friends.

ACKNOWLEDGMENTS

Special thanks to Dr. Zhengdong Cheng for his unending guidance, support and encouragement in completing this thesis. I also thank Dr. Ali Beskok and Dr. Debjyoti Banerjee for their advice and encouragement as my committee members. I confess I couldn’t do this work without the help of my colleague, Dr. Dawei Luo. He is always open to any questions and discussion. I also thank ICF friends, Luo Wen, Bill and Bel, Kent and Judy. I have felt at home because of their love, friendship and guidance. And I am always grateful to my family in Korea for their support and love. Finally, I want to thank God for everything.

TABLE OF CONTENTS

Page

Page

LIST OF FIGURES

Page

NOMENCLATURE

Q_i	Inner flow rate
Q_o	Outer flow rate
d	Diameter of droplet size
V	Voltage
P	Static pressure
$\bar{\tau}$	Stress tensor
ρ	Density
$\vec{g}$	Gravitational acceleration
$\vec{F}$	Force at the surface by surface tension
σ_{ij}	Surface tension between i and j phases
$\vec{v}$	Velocity vector
k_i	Curvature of the i phase
α_i	Volume fraction of the i phase
μ	Viscosity
I	Unit tensor
$\dot{m}_{pq}$	Mass transfer from phase p to phase q
$\dot{m}_{qp}$	Mass transfer from phase q to phase p

CHAPTER I

INTRODUCTION

1.1 Background and Research Objective

The technology of emulsion drop generation becomes popular with its wide application in food industry, cosmetics, drug delivery and ink jet printer. Microfluidic technology is at the frontier of the development of controlled emulsification[1]. Flow focusing geometry[2] is commonly used to generate droplets, whose size readily controlled by the flow rate ratio. Anna et al. used the mode of breakup, so called tip-streaming, to generate tiny droplets which are a few micrometers in size[3]. However, there are limits to control the droplet size by changing the geometry, size of the channels and the properties of the fluids. On the other hand, the electrospray is an ionization and disintegration technique of droplets in a high electric field, which has a wide range of applications including mass spectrometry of macro-molecules[4]. It is a physical process caused by an electric force applied to a liquid surface. Many experiments have been carried out to make small droplets using electrospray. Bose first reported the electrohydrodynamic spraying from the electrified capillary in 1745[5]. In 1882, Rayleigh established a stability criterion for electrified droplets[6]. After several years of investigation, Zeleny made a pioneering systematic investigation of the discharge from

---

This thesis follows the style of *Physics of Fluids.*

the electrified water surface in 1917 [7]. Vonnegut and Neubauer computed the equilibrium value for the droplet radius by the minimum energy method in 1952 [8]. In 1964, Taylor described the cone-jet mode which has semi-vertical angle of 49.3°, which later bears his name [9]. Mutoh studied disintegration of a viscous jet with various conductivities in 1978 [10]. In 1986, Hayati et al. explained the mechanism of an electrospray using the electrical shear stress [11].

Figure 1 illustrates the most commonly used electrospray setup. A liquid is supplied by the pump through a capillary tube. The electrode is inserted in the capillary tube which contacts the liquid. The electric field is formed between the liquid tip and the metal plane which is grounded. The distance can be adjusted to control the electric field strength. The electric field is always perpendicular to the metal plane. The droplet sizes are mainly controlled by the flow rate of the liquid, diameter of the capillary tube and strength of the electric field.

Most of the experiments have been conducted in the spray of a liquid in a gas. Only a few experiments of emulsification in the electric field have been performed so far with a liquid in an immiscible liquid. In 1997, Sato proposed a method to form droplets in water and explained electrohydrodynamic flow in macroscopic scale [12], but the device was not able to electrospray. Barrero et al. made cone-jets of conducting liquids inside insulating liquids which were stationary [13].

In this thesis, the electrospray in a flow-focusing microfluidic emulsification device was carried out. For flow-focusing microfluidics, droplet size depends on the size of the device, geometry, properties of the fluids and flow rates of inner (Q_i) and outer

fluids (Q_o) , which can produce droplets down to micrometer sized [2] . Typically, droplets are produced with a narrow size distribution (~2%). The electric field offers another dimension to control droplet size, and possible to generate submicrometer droplets.

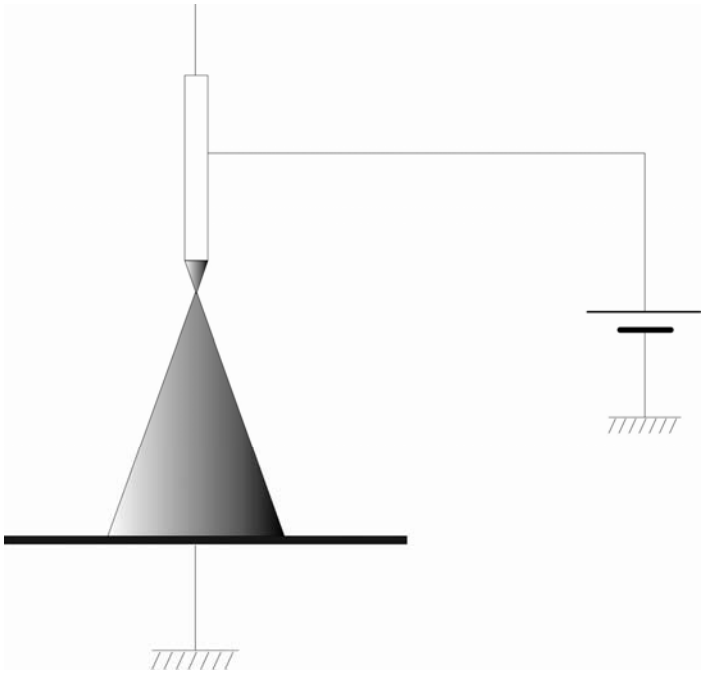

Fig. 1. Electrospray in air.

Specifically, we shall control the droplet size using the electric field, and also investigate the effect of AC voltage. Using the commercial CFD package, the period II (a series of the generation of big and small droplet) in flow focusing configuration will be analyzed to explain the phenomenon.

CHAPTER II

DROP PRODUCTION IN FLOW-FOCUSING MICROFLUIDICS WITH ELECTRIC FIELD

2.1 Experimental Setup

2.1.1 Flow-Focusing Microchannels

The flow focusing geometry is used to generate droplets in microchannels as shown in Figure 2. It can form micro-sized droplets (10-100 μm size in diameter) close to the size of the orifice with a narrow size distribution[14]. The fluid is driven by syringe pump. The Cross section of the channels is typically rectangular.

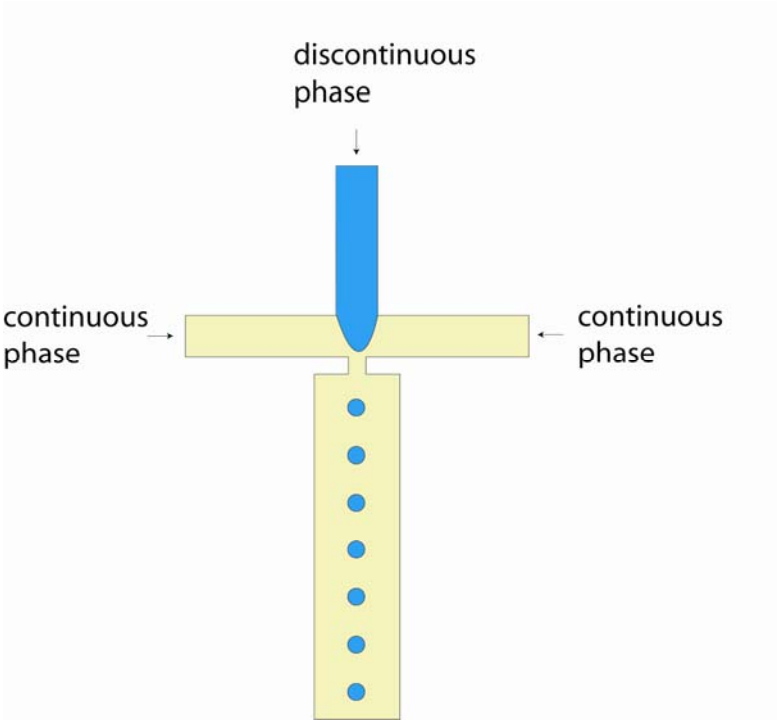

Fig. 2. Flow-focusing geometry.

Deionized water is used as the dispersed phase which flows through the central channel. Mineral oil with a span 80 (Sorbitan monooleathe, SIGMA, St. Louise, MO) as surfactants (6 wt%) was used as the continuous phase which exerts shearing force to the water tip. Droplets were generated inside the orifice. The dispersed phase was always surrounded by the continuous phase and has less tendency to wet the walls of the channels than the continuous phase. Oil flow rates were normally higher than water flow rates to create a reasonable conic water tip. Drop sizes and the patterns of an assembly of droplets were controllable by the ratio of flow rates of inner to outer fluids[2]. They were also affected by the size of the channel and geometry. Smaller orifices can generate smaller droplets in the identical operation. Droplet production frequency is in the order of 1kHz, so the production was captured using high-speed CCD camera (Phantom V4.2, Vision Research, Wayne, NJ) up to frame rate of 2200 fps.

2.1.2 Syringe Pumps

The fluids were driven by syringe pumps. We used a modified syringe pump (PHD2000, Harvard Apparatus, Holliston, MA) as shown in Figure 3 to generate stable flow at very small flow rate under 10ul/h[15] because there was a fluctuation in flow rate when the rate was small using the 1.8° stepper motor of the unmodified syringe pump. The step motion of the motor goes much smoothly via a reducer. A 100.56:1 speed reducer (Berg, East Rockaway, NY) was connected to the drivescrew. While the motor turns 100.56 times, it generates a turn of the drivescrew via the speed reducer. So, the

drivescrew connected to the syringe pump can develop much smoother movement of the fluid.

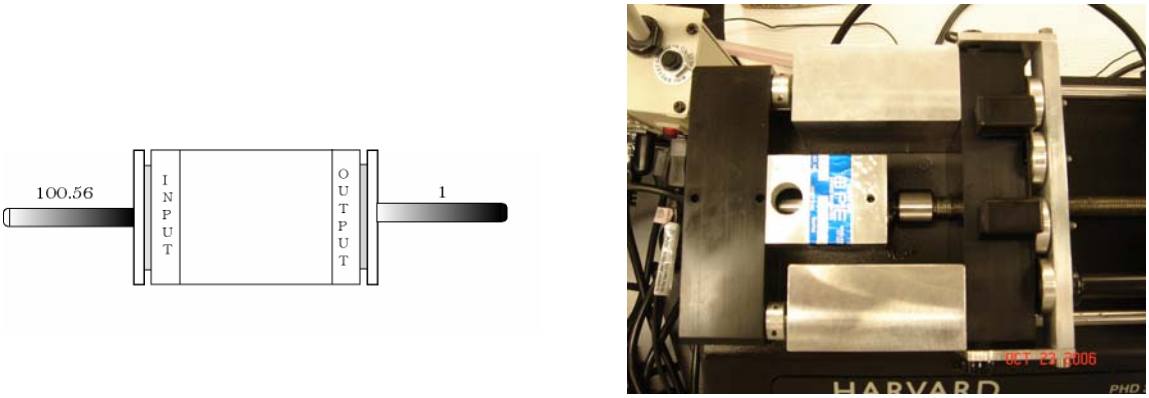

Fig. 3. Modified syringe pump with speed reducer. Speed reducer is connected to the drivescrew of the pump.

2.1.3 Soft-lithography[16]

The device was fabricated by soft lithography. It is a cheap and convenient method to make microfluidic devices. The following is the general procedure (Figure 4). We first draw the microchannels using Adobe Illustrator CS (Adobe) which is used as the photomask when printed on a transparency at high resolution. The rest of the procedures were done in the clean room. The silicon wafer was chemically cleaned, which was used as a substrate. Then it was put in the reactive ion etching (RIE) chamber for the ion plasma etch. We then dried it on hot plate for 5 minutes of $120^{\circ}C$. Su-8 2050, a negative photoresist, covered with the wafer on the spin coater, and the thickness was set by the spin speed. The typical speed is 2000rpm for a $75\,\mu m$ height channel. After the photoresist was applied to the wafer, it was baked on a hot plate at $95^{\circ}C$. The UV light polymerized the photoresist using the mask aligner.

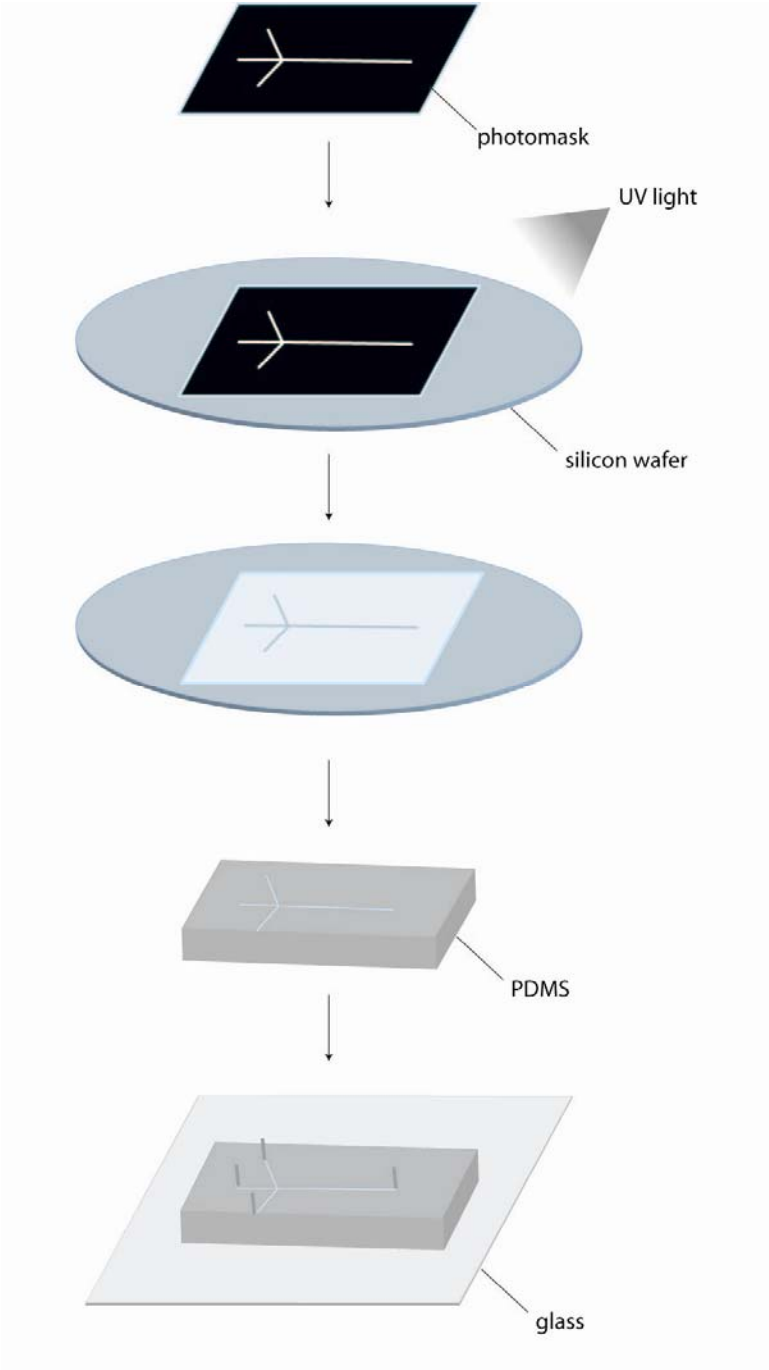

Fig. 4. Schematic of device fabrication.

Only the UV exposed area became polymerized, the rest of the photoresist was washed away during the development step. The wafer needed to be baked again before we put it into the Su-8 developer. After the clean room work, we transfer the designed pattern from the mask in the Su-8 photoresist onto a silicon wafer. We put the patterned wafer in a petri dish, which was filled with the PDMS (polydimethylsiloxane). The mixture (the mixing ratio of the PDMS to crosslinker is 10:1) was vacuumed to get rid of air bubbles. And we baked it in the oven at $60^{\circ}C$ for 1 hour. After that, the PDMS was peeled off with the duplicated photoresist pattern on it. We, then, made holes for the inlets and outlet. And we went to the clean room again to put it in the RIE for the oxygen plasma etching with a glass slide which sealed the channels by bonding the PDMS chip with the glass slide.

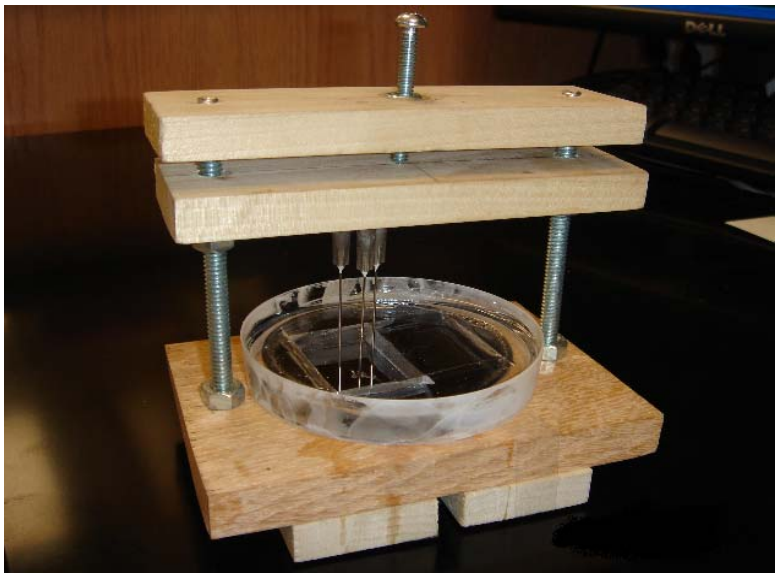

Fig. 5. Device for holding the pin.

After several times of use, the PDMS was swollen by having absorbed the oil. So it needed to be replaced with new PDMS. After several experiments, the channels were easily clogged by the debris from the holes punched in the PDMS (polydimethylsiloxane) using modified syringe needles. To get rid of the debris, water was flushed through the inlet channels for several hours before the PDMS was attached to the glass. Then, the majority of the debris was washed out of the holes. In addition, instead of puncturing the PDMS, pins were directly glued to the substrate. It made clean holes but the glue permeated through the channels which, in turn, blocked their flow. To solve this problem, we made a device (Figure 5) which held the pins without glue. We also designed filters (Figure 6) in each inlet that had a smaller width than the channels. Therefore, the debris could not enter the channels.

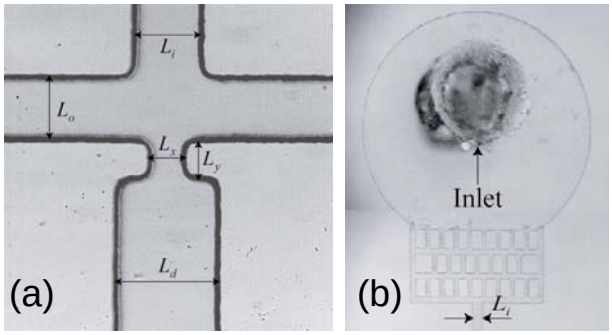

Fig. 6. Microimage of the microfluidic device. (a) Flow-focusing geometry. $L_i = L_o = 100\mu m$, $L_d = 150\mu m$. The orifice size is $L_x = L_y = 50\mu m$. (b) Microimage of the filter. Filters are located at each inlet to prevent clogging.

Using a combination of these methods, the channels can be cleared even more effectively. Channels were coated by Aquapel (PPG Industries, Inc., Pittsburgh, PA) to prevent water droplets from wetting the PDMS walls. The coating makes the glass of the

inside channels more hydrophobic. The height of the channels was about 61.4 μm as measured by the profilometer. The liquid should be semiconducting in order to form a Taylor cone. If the liquid has a high conductivity, it cannot form a Taylor cone because there would be no potential difference in the liquid[11]. The conductivity of the deionized water in our experiments was 0.378 μS .

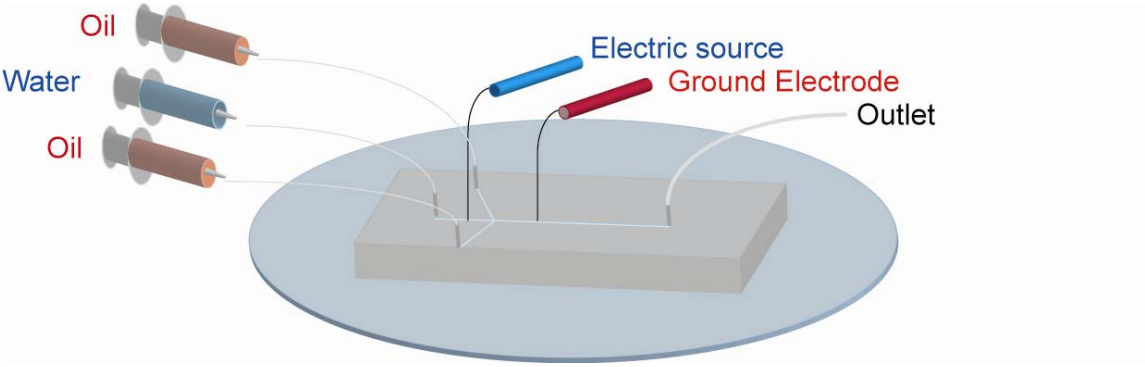

Fig. 7. Illustration of the device.

Figure 7 shows the schematic of the device. The electric source and the ground electrode were inserted to the PDMS and they contacted the fluid inside the channels, which generated the electric field between the electrodes. The electric field is dependent on the distance between the electrodes (365μm) as well as the applied potential difference. The formation of a Taylor cone is necessary to generate very fine droplets. When the electric field is applied to the channel, the water-oil interface on the tip is charged, which behaves like a capacitor.

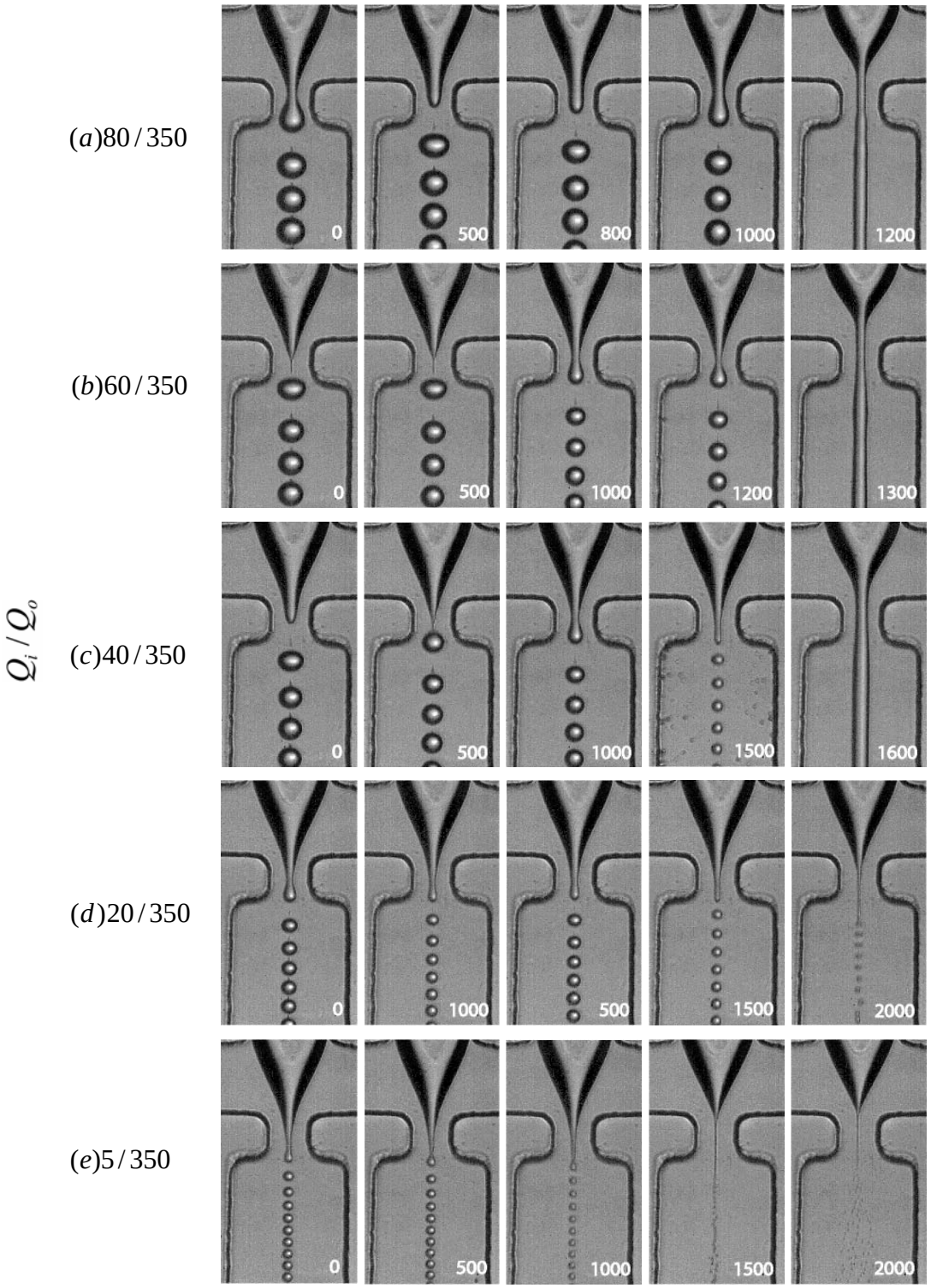

Fig. 8. Phase diagram of droplet generation in DC electric field. The row represents the different flow ratio of inner and outer fluid flow (Q_i / Q_o). The number at the corner of each micrograph represents the applied voltage.

As the voltage increases, the charges on the interface increase introducing higher attraction towards downstream. The tip of the Taylor cone is stretched to a narrow filament and is broken into tiny droplets due to the Rayleigh instability[17]. Smaller droplet size was produced at smaller flow rate ratio (Q_i / Q_o) of dispersed flow rate to continuous flow rate at the same voltage. Smallest droplets under 1 μm in diameter were produced when the tip formed a Taylor cone as shown in Figure 8(e). Low flow rate ratio as in case (e) is necessary to form the Taylor cone. The electric field barely affects the droplet size at high flow rate ratio such as case (a). It formed jetting at 1200V, which could not generated droplets. Because of the jetting, we could not get a Taylor cone at any voltage.

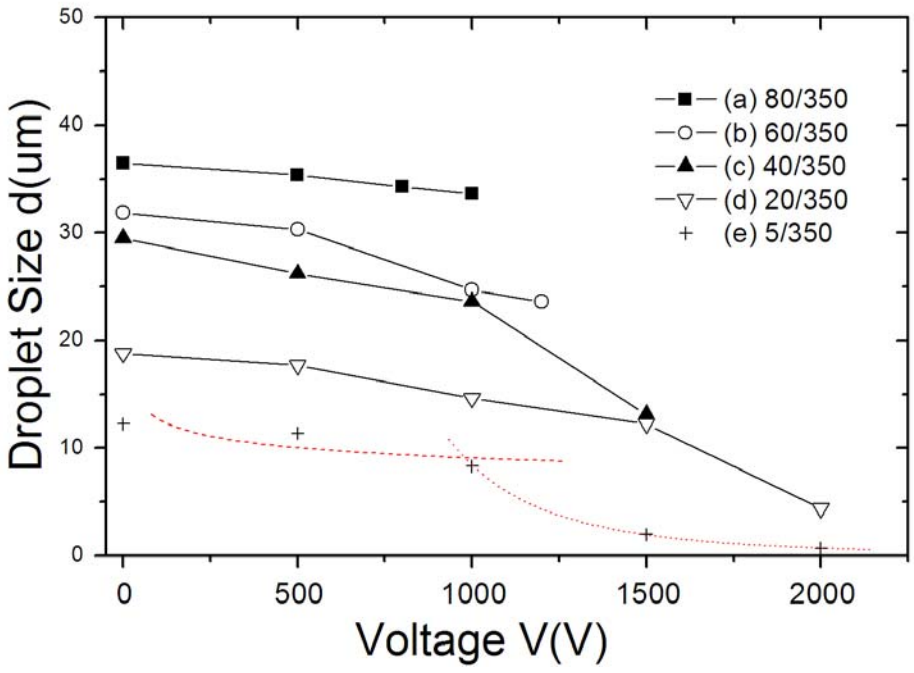

Fig. 9. Drop size in function of voltage. Drop size depends on voltage and flow rate ratio, which quantitatively describe the dependence of drop size on voltage and flow rate ratio. The data for case (e) are fit to two power functions.

While the electric filed is applied, the droplets deformed (stretching in the electric field direction) and enhanced coalescence was observed. Jetting mode appears at the high voltage and high flow rate ratio. The tip of water stretched bridging the ground and no longer generated droplets.

The quantitative information of Figure 8 was extracted by image analysis and plotted in Figure 9. At large ratio the size are the order of the orifice. Decreasing the flow rate ratio, the size can reduce half an order of magnitude by flow focusing. Case (e) shows another order of magnitude can be achieved using electric field. Electrospray via Taylor cone was observed for case (a) above 1500V. Drop size was related to voltage as $d \sim V^{-0.2}$ at low voltage where the flow focusing dominates and $d \sim V^{-3.6}$ at high voltage when electric field dominates over the shear force. The cross over voltage for case (e) is 1000V (the corresponding field strength is $2.7V/\mu m$). The channel width after the orifice should be narrow to increase the distance between droplets.

2.2 AC Electrospray

2.2.1 Phase Diagram in the Voltage-Frequency Plane

Figure 10 shows the effect of the voltage and the frequency. The voltage does not have a big effect on the droplet size when it is low, which has shown a stable dripping mode at any frequency. Interestingly, the jetting mode came back to dripping mode at high frequencies. To generate the stable Taylor-cone, the voltage and the frequency should be in the proper range (stable Taylor cone region are shown by triangles in Figure 10).

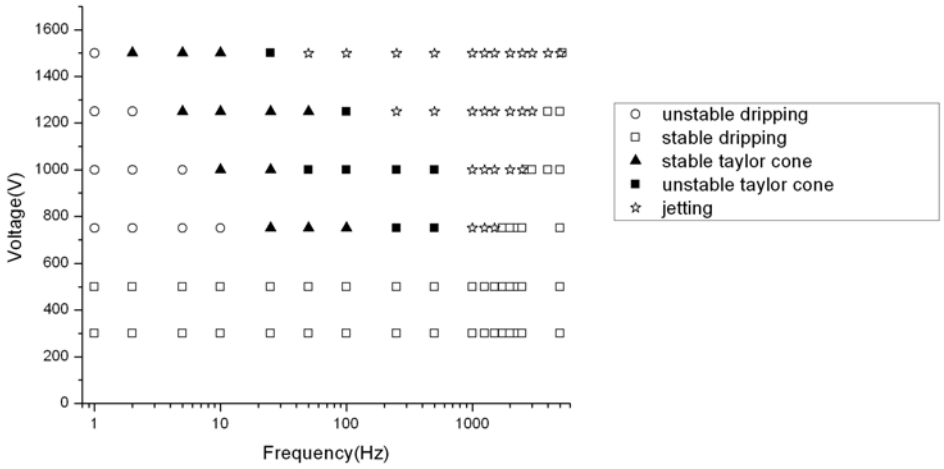

Fig. 10. Modes of electrospray in hydrodynamic flow focusing with rectangular waveform. (Q_i / Q_o : 20/300)

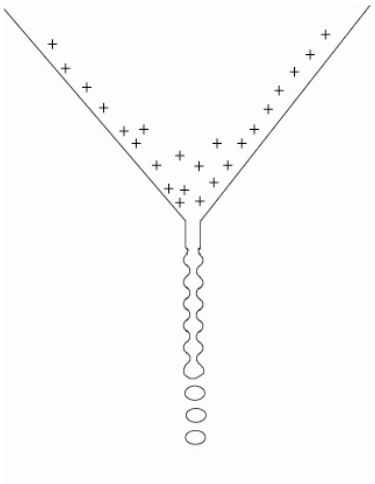

Fig. 11. Formation of fine droplets in a Taylor cone. The tip is pulled by electric forces and elongated tip dissipates into small droplets.

Formation of a Taylor cone (Figure 11) is necessary to generate very fine droplets. When the electric field is applied to the channel, the water-oil interface on the tip is charged, which behaves like a capacitor[18]. As the voltage increases, the charges on the interface increase introducing higher attraction downstream. The tip of the Taylor cone is stretched to a narrow filament and is broken into tiny droplets due to the Rayleigh instability[17].

Barrero et al. produced the Taylor-cone by conducting liquids inside insulating liquids which are stationary[13]. But after generating the droplets, it was hard to collect them from the bath due to the high possibility of droplet coalescence. Therefore, we used a flow-focusing geometry, which makes the droplets more suitable for collection. However, the longest time we observed the Taylor cone was about one minute in DC electric field.

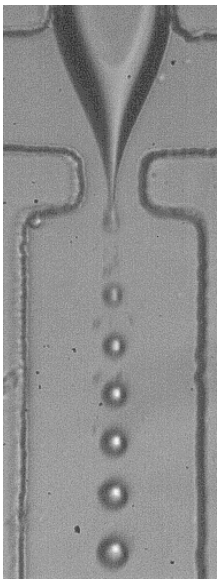

Fig. 12. Breakup of different sized droplets.

We used 10Hz triangular waveform to see the simultaneous effect of applied voltage on droplet size. Droplet size changed smoothly as the voltage increased (Figure 12). Each droplet has different size according to the applied voltage.

We generated various waveforms to observe the effect of voltage using a function generator (DS345, Stanford research systems, Sunnyvale, CA). Its amplitude was the maximum part of the waveform, which was controllable. When the voltage reached a threshold voltage, the tip became a Taylor-cone and kept it while the voltage was larger than the threshold.

2.2.2 Rectangular Waveform

We used a rectangular waveform to see how the voltage affects the size of the droplets. The voltage was 1000V with a frequency of 3.64Hz. Figure 13 shows the droplet size as a function of voltage. When the voltage was zero, the droplet size was the largest. In general, as the voltage increased, the size of the droplets decreased. There was a fluctuation when the voltage got to 1000V. Even though the voltage remained the same as 1000V, the droplet size increased. And it maintained at a certain size of droplets until the voltage started to decrease. At 0.025s, there was a fluctuation again, then the droplet size increased until it got back to the maximum size and completed the period.

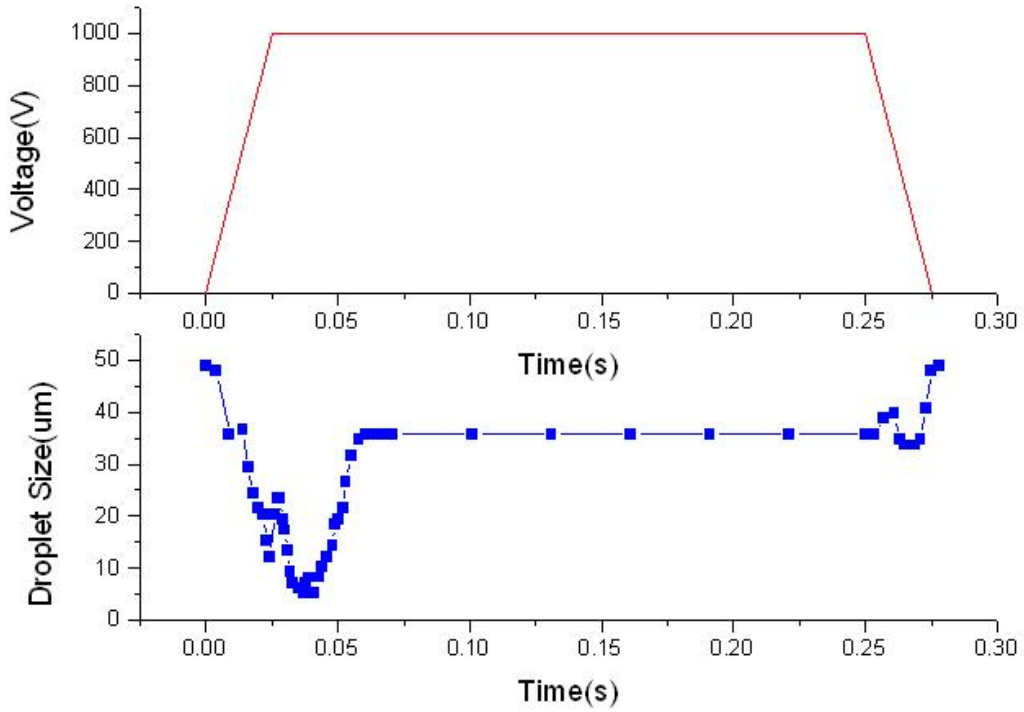

Fig. 13. Voltage and droplet size as a function of time with rectangular waveform.

As the voltage increased, the tip position of the water became longer, which produced small droplets with a high rate. At this moment, the emitted flow rate from the tip was larger than the supplied flow rate from the water pump. After a while, the volume of emission became the same as the volume of supply. Therefore, tip became stable and generated uniform size droplets. Figure 14 shows the change of the tip shape at 0 and 1000V.

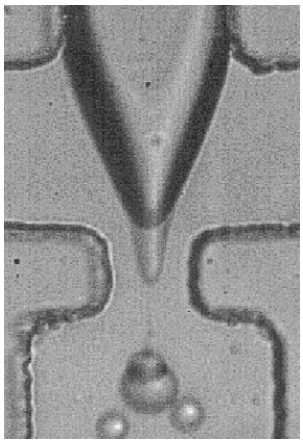

Fig. 14. Overlay of the tip at the voltage of 0 and 1000V.

2.2.3 Triangular Waveform

We used the triangular waveform (Figure 15a) to see how the voltage affects the size of the droplets. The voltage was 750V with a frequency of 10Hz. When the voltage was zero, the size of the droplet was the largest. In general, as the voltage increased, the size of the droplets decreased. The droplet became the smallest at around 580V. Even though the voltage increased to 750V, the size increased. This is because the water in the tip did not have enough fluid to form electrospray. Therefore the tip moved back a little bit to have long enough time to make droplets. So even though the voltage increased, it generated big droplets. There was also some fluctuation when it came back to zero voltage. It is also explained by the same mechanism. At 490V the size started to decrease while the tip had enough fluid. Finally it came back to the largest droplet and completed the period. Figure 16 shows the effect of symmetric triangular waveform on droplets.

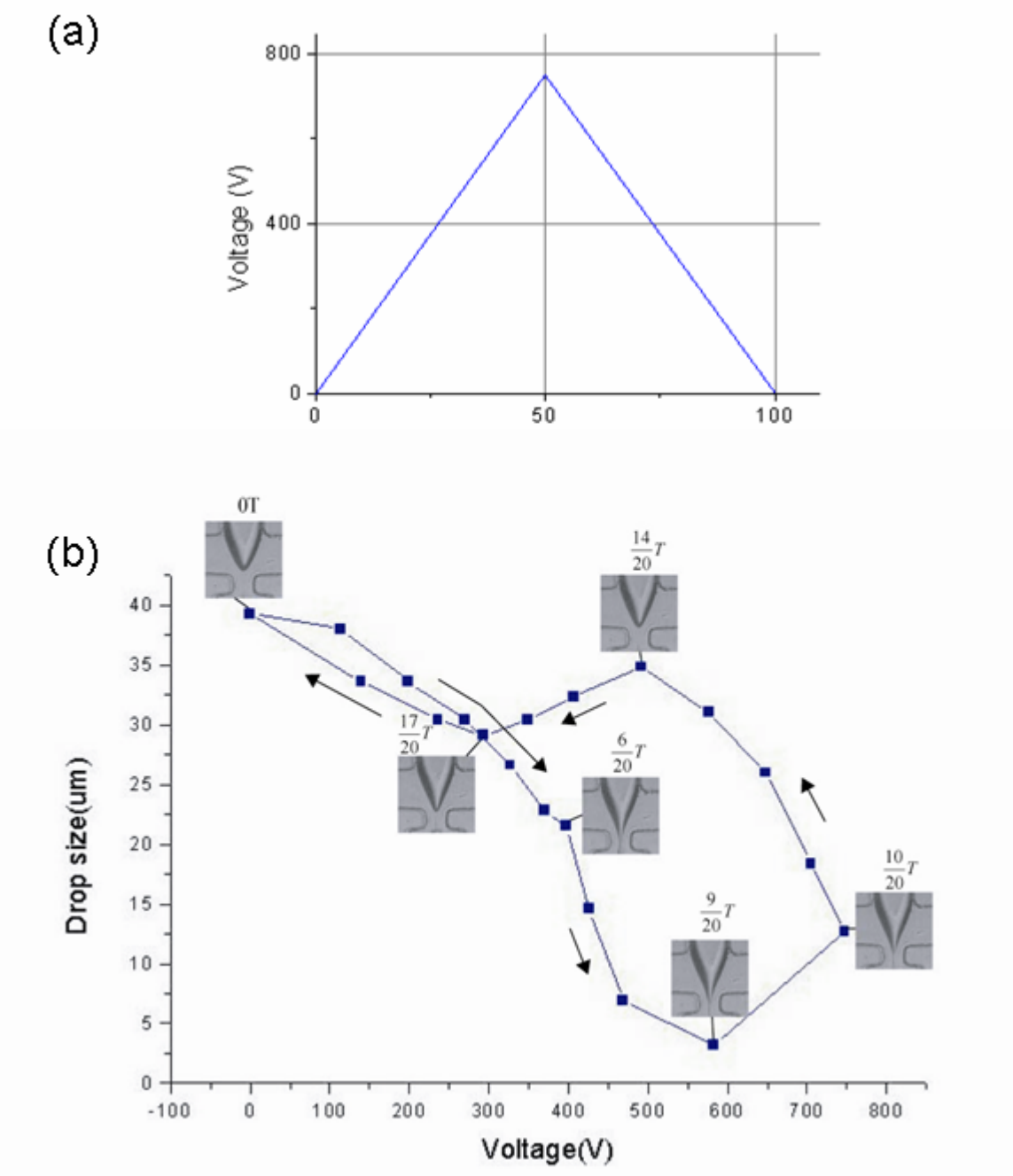

Fig. 15. Voltage and droplet size as a function of time with triangular waveform. (a) Positive triangular waveform with 10Hz (Q_i / Q_o : 20/300). (b) Change of tip shape with the applied voltage.

Threshold voltage is defined as the lowest voltage which generates a Taylor cone. The round shape of tip is transformed to sharp jet emitting tip at the threshold voltage. In flow-focusing geometry, the tip of the water is very sharp even without an electric field due to the shearing force by the outer fluid. So there is no clear transition to the threshold voltage. Therefore, it is hard to tell the exact value of the threshold voltage.

The size of droplets is related to the position of the tip as shown in Figure 17. If the tip position is low, it generates small droplets. If the tip position is high, it generates big droplets. The tip position is affected by the voltage and the water feed rate with the fixed outer oil flow rate. To lower the tip position and generate small water droplets, there should be enough water feed rate and high enough voltage.

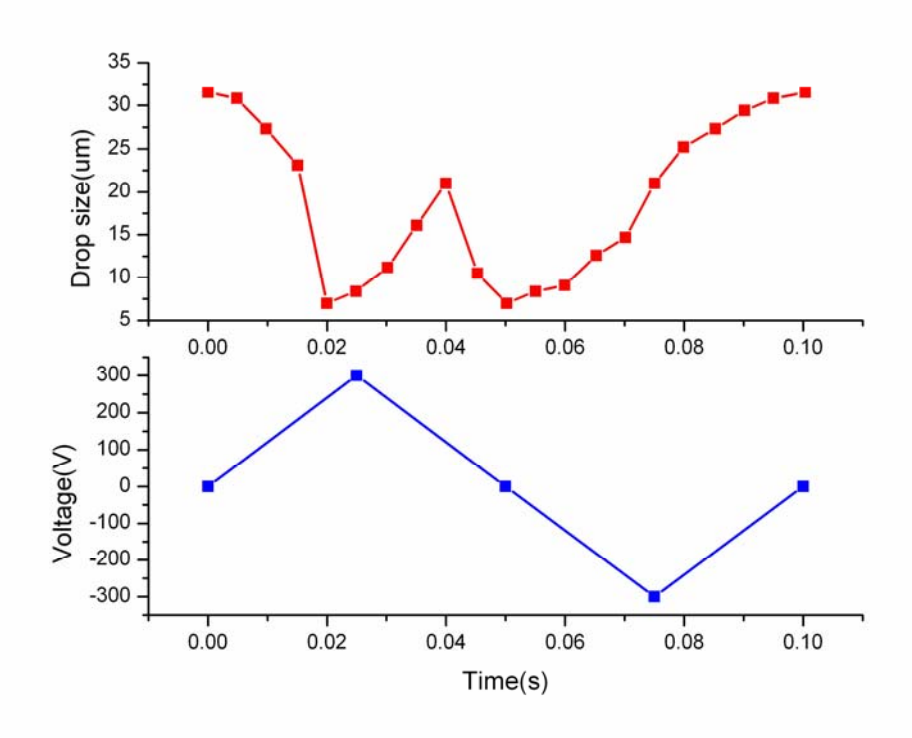

Fig. 16. Symmetric triangular waveform with 10Hz (Q_i / Q_o : 20/300).

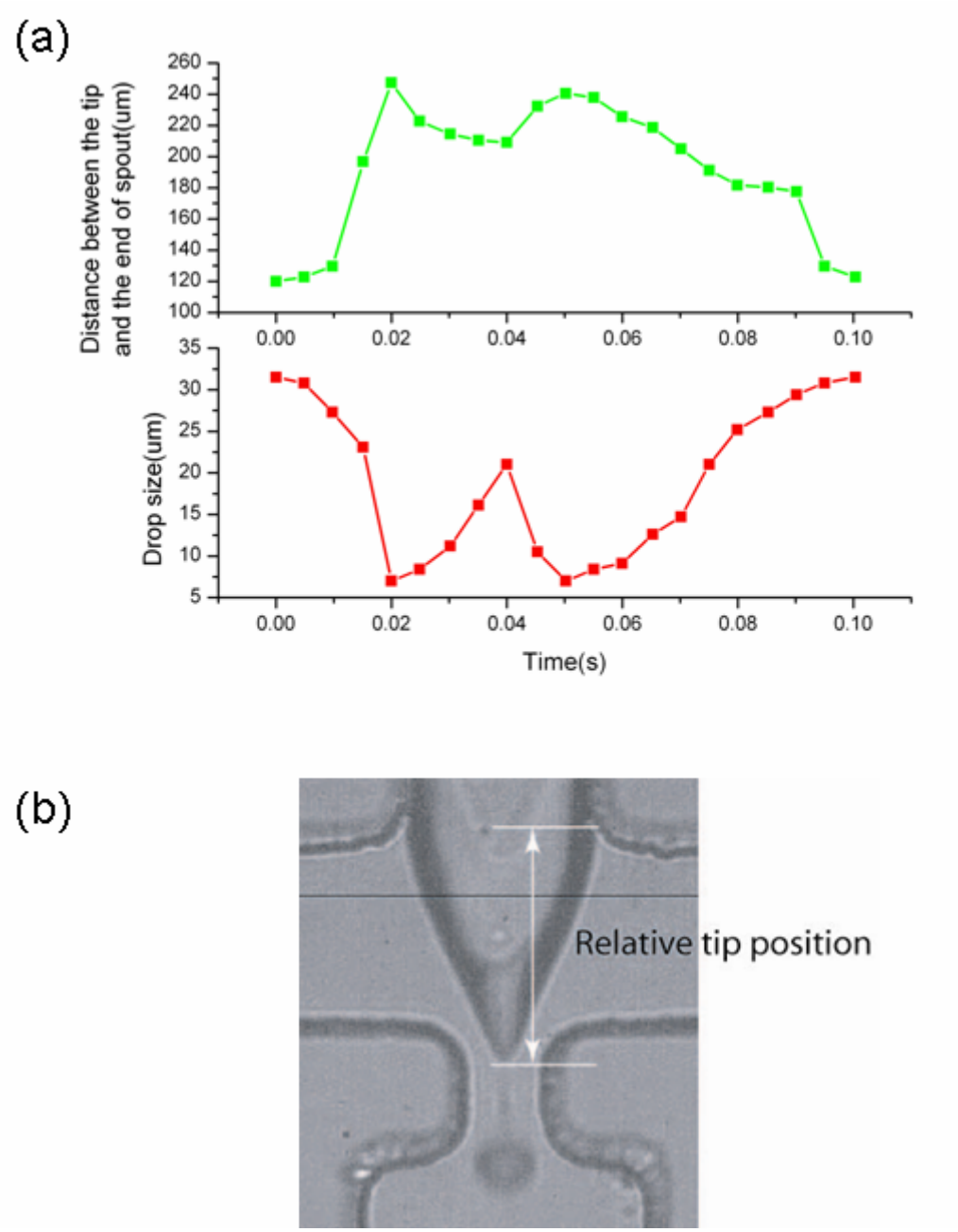

Fig. 17. Tip position and the droplet size. (a) Plot of tip position and the droplet size with time (b) Microimage of the channel showing the relative tip position.

2.2.4 Electric Field in the Channels

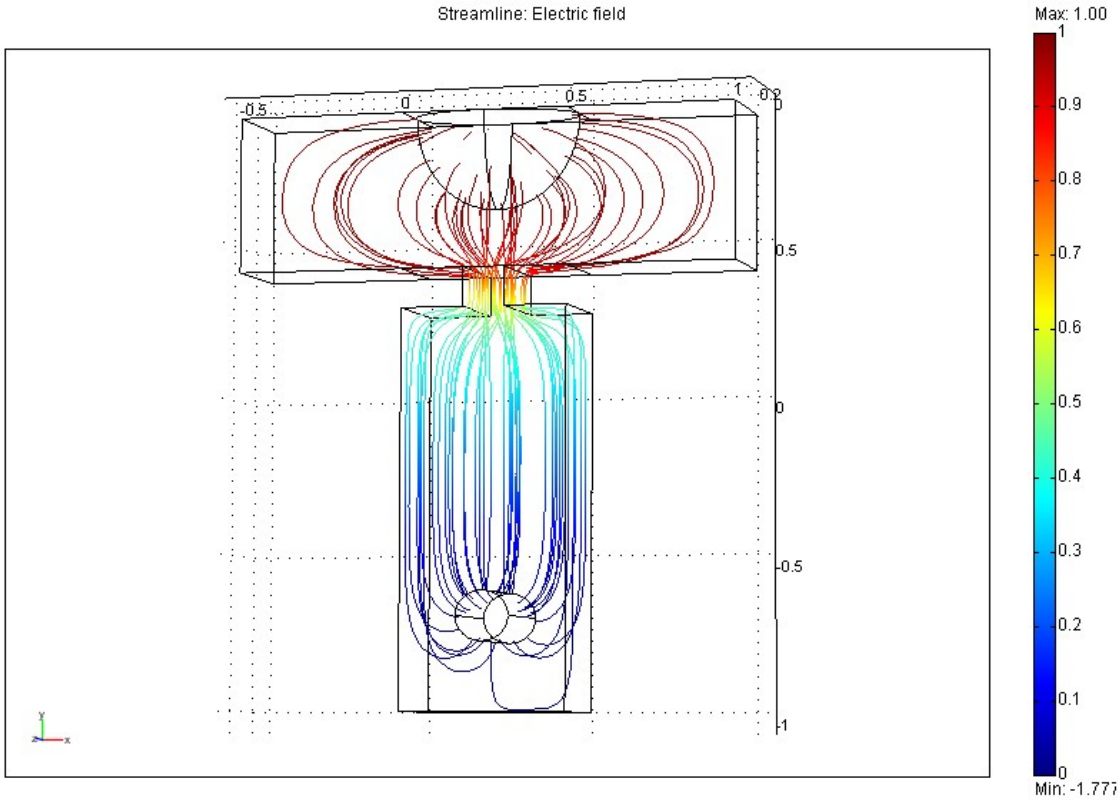

Fig. 18. Electric field distribution in flow focusing using FEMLAB.

Electric field was calculated to see the how it controls the droplets precisely in the channels as shown in Figure 18. At the top of the channels it had a water tip which had electric potential the same as the voltage we put in the function generator. The hole at the bottom was the wire which was grounded. The electric field was the strongest in the orifice which had the smallest cross section in the channels. The electric field lines were always perpendicular to the surface of the tip. In the experiment, there were outer

flow and charged droplets between the electrodes which would vary the shape of the electric field lines slightly.

CHAPTER III

SIMULATIONS OF BIMODAL DROP PRODUCTION

3.1 Background and Simulation Setup

Two papers of simulation for drop production in flow focusing have been published in recent years. The dynamics of drop formation was predicted as a function of the Reynolds numbers and Weber numbers [19]. And the compound drop formation and the viscoelasticity effect in the drop phase were investigated [20]. At some flow rates, the microfluidic device generated a bigger droplet followed by a smaller one consecutively, which is defined as period 2 as shown in Figures 19 and 20.

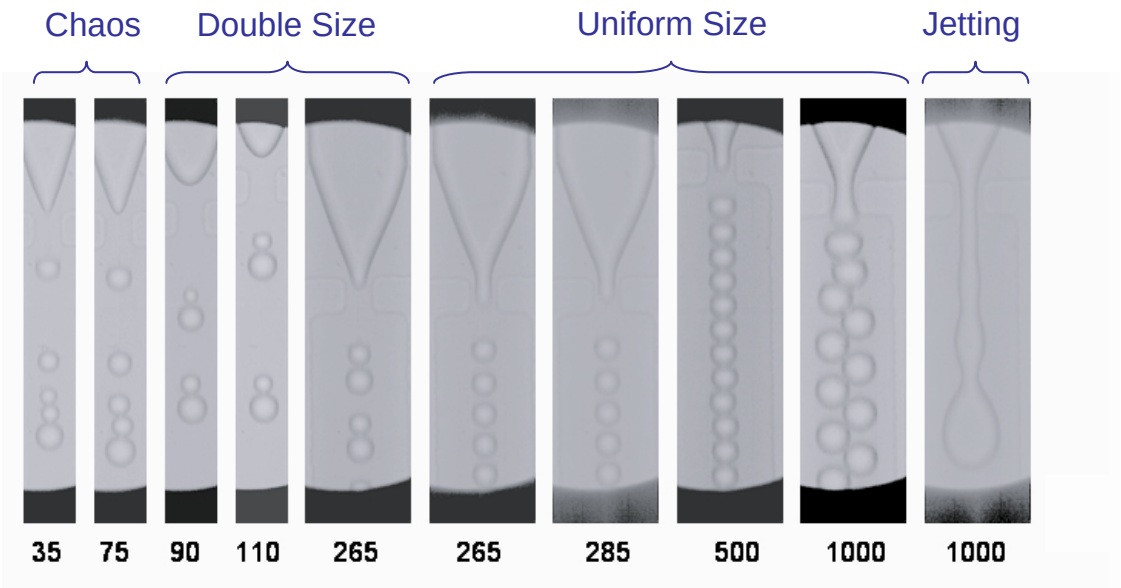

Fig. 19. Micrographs of drop production modes [21]. Water flow rate ($\mu l / h$) changes while the oil flow rate is fixed to 1000 $\mu l / h$.

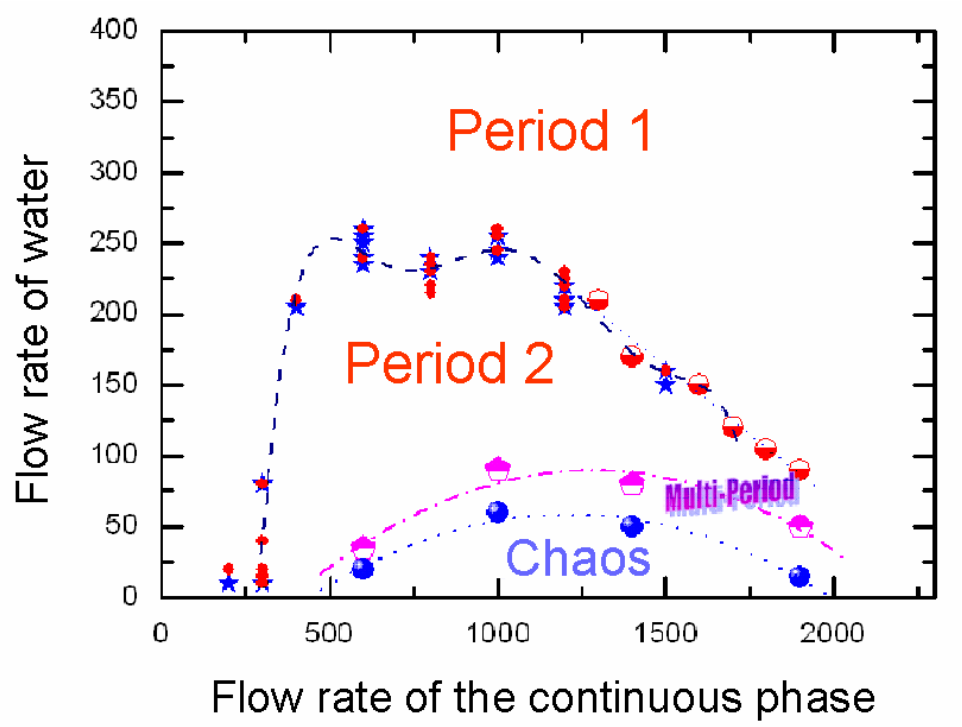

Fig. 20. Phase diagram of drop production modes[21]. Symbols represent experimental data. Monodisperse droplets are generated in period 1. Randomly sized droplets are generated in chaos regime. Units of the flow rate are $\mu l / h$.

To understand this instability of drop formation, a numerical calculation was conducted in flow focusing geometry using FLUENT. This study focused on analyzing the droplet formation of period 2. The volume of fluid (VOF) model was used to track the interface between the two phases. The qualitative correlation between the experiments and simulations was observed. The geometry of the device was two dimensional and drawn by GAMBIT as shown in Figure 21. In the middle of the channel, the discontinuous phase was flowing. At both sides of the channels, the continuous phase was flowing. The continuous phase never touched the walls. All of the walls had

non-slip boundary conditions. The motion of the fluid was governed by the Navier-Stokes equation.

$$\frac{\partial}{\partial t}(\rho\vec{\upsilon})+\nabla\cdot(\rho\vec{\upsilon}\vec{\upsilon})=-\nabla p+\nabla\cdot(\bar{\tau})+\rho\vec{g}+\vec{F} \tag{1}$$

$$\vec{F}=\sigma_{ij}\frac{\rho\kappa_i\nabla\alpha_i}{\frac{1}{2}(\rho_i+\rho_j)} \tag{2}$$

$$\bar{\tau}=\mu\left[(\nabla\vec{\upsilon}+\nabla\vec{\upsilon}^T)-\frac{2}{3}\nabla\cdot\vec{\upsilon}I\right] \tag{3}$$

where p is the static pressure, $\bar{\tau}$ is the stress tensor, $\rho\vec{g}$ is the gravitational body force and $\vec{F}$ is the force at surface by surface tension.

The gravity term was disregarded because it was very small. α is the volume fraction of the phase to track the interface between the immiscible fluids. Two phase systems were used in the simulation.

$$\alpha\begin{cases}0 & \text{fluid is empty in the cell}\\ 1 & \text{fluid is full of the cell}\\ 0<\alpha<1 & \text{cell has an interface between the two fluids}\end{cases} \tag{4}$$

The interface between the two fluids can be traced by the following continuity equation.

$$\frac{1}{\rho_q}\left[\frac{\partial}{\partial t}(\alpha_q\rho_q)+\nabla\cdot(\alpha_q\rho_q\vec{\upsilon}_q)=\sum_{p=1}^{n}(\dot{m}_{pq}-\dot{m}_{qp})\right] \tag{5}$$

The sum of volume fraction is

$$\sum_{q=1}^{n} \alpha_q = 1 \tag{6}$$

The properties of each phase can be calculated by the volume fraction α .

$$\rho = \alpha_2 \rho_2 + (1 - \alpha_2)\rho_1 \tag{7}$$

$$\rho = \sum \alpha_q \rho_q \tag{8}$$

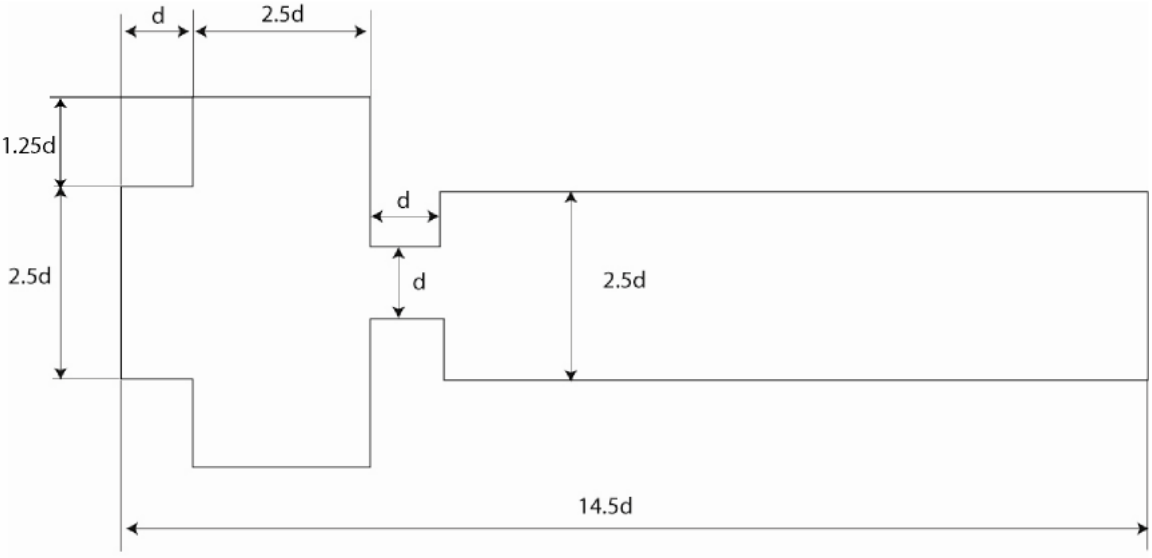

Fig. 21. Schematic of the flow-focusing geometry.

3.2 Simulation Results

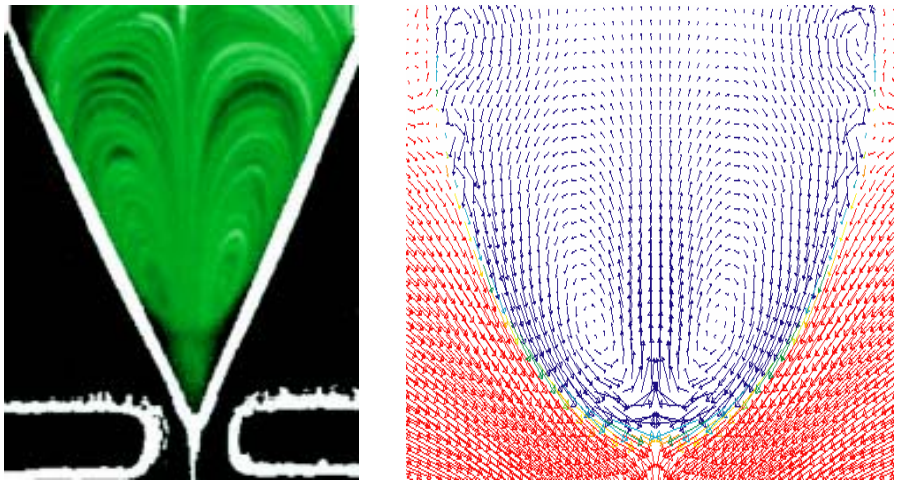

Fig. 22. Circulation pattern in the conical base of continuous phase. Experimental result(left) [9], velocity profile inside the tip from the simulation result.

The simulation results corresponded to the experimental results. The flow inside the conical base of the continuous phase (water) circulated as shown in Figure 22. The velocity on the surface of the tip was the greatest. After it reached the apex of the tip, it went back to the base and circulated.

Two sets of simulation were carried out with the same conditions except the surface tension and flow rate ratio. The viscosity ratio for both simulations was $\mu_i / \mu_o = 0.001003 / 0.006018$. In the first set of simulation, the surface tension and the flow rate ratio were 0.020N/m and $Q_i / Q_o = 1/9$. In the second set of simulation, the surface tension and the flow rate ratio were 0.015N/m and $Q_i / Q_o = 1/8$. In simulation 1, monodisperse droplets (in Period 1) were generated, as shown in Figure 23. The inner fluid was focused by the outer fluid and stretched into a filament. The end of the

filament increased gradually, which formed a bulb and the breakup occurred in the neck. After the pinch-off, the tip retracted to the original position and commenced a new cycle.

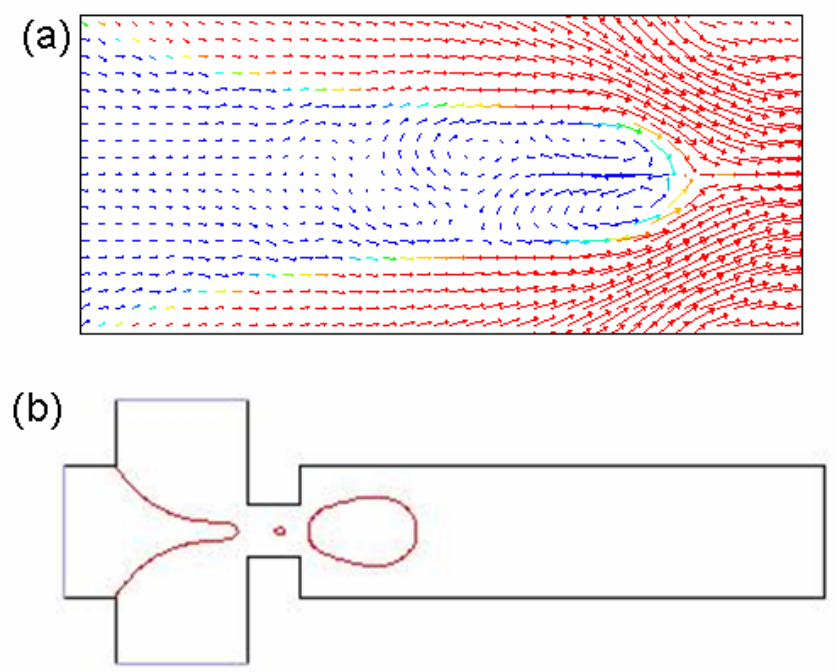

Fig. 23. Velocity profiles of tip and snapshots of drop formation in Period 1. (simulation 1)

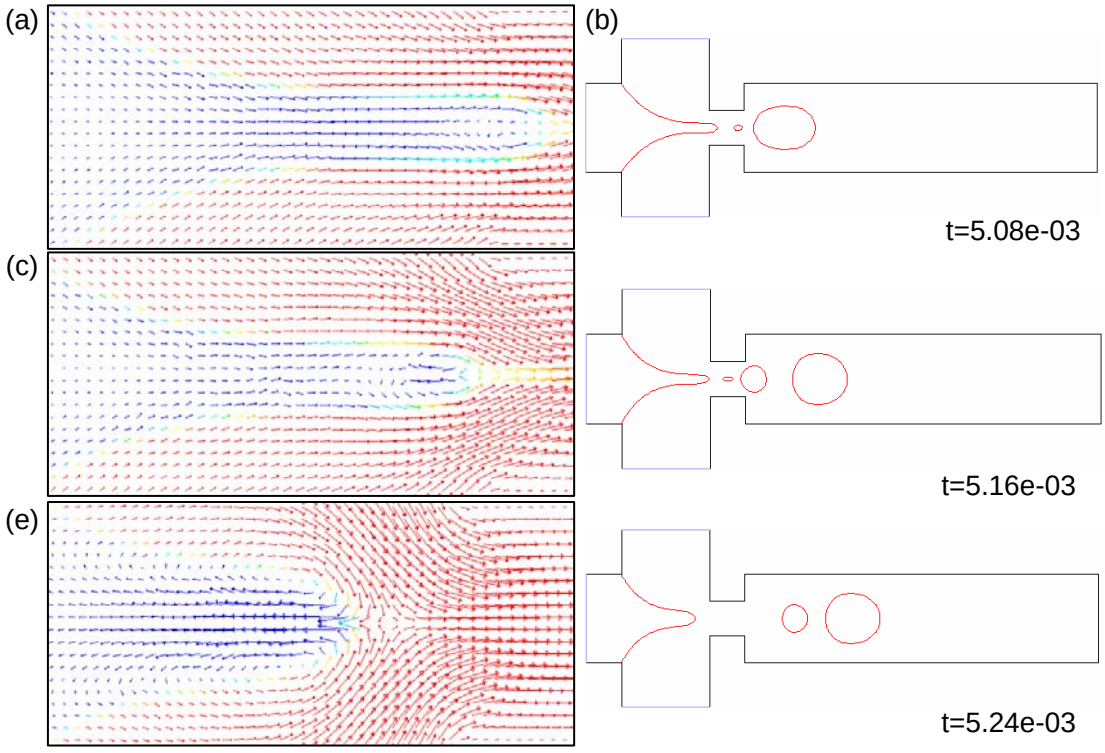

Fig. 24. Velocity profiles of tip and snapshots of drop formation in Period 2 with time. (simulation 2)

In simulation 2, droplets in Period 2 were generated, as shown in Figure 24. The velocity profiles of both cases were compared to observe the differences between them. After a big droplet was generated, the tip retracted to the orifice. However, the tip did not move back to the original position as it generated uniform size droplets. The tip grew again and generated another smaller droplet. After generating two droplets, the tip returned to original position to start over a new cycle.

CHAPTER IV

CONCLUSIONS

Droplet size is able to be controlled by the electric field in microchannels. Typically, the droplet size decreases as the voltage increases. At low voltage and large flow rate ratio, the size is solely determined by hydrodynamic flow focusing. Electric field can sensitively control the droplet size only at small flow rate ratio with low flow rate of the dispersed phase. The droplet size produced via the Taylor cone is less than $1\ \mu m$. There is a force balance at the tip among the electric force, the capillary force and the surface tension. The charges stay on the surface of the tip, which is pulled over by the electric field. The outer fluid exerts shear force on the tip. The tip stretches to the narrow filaments and causes droplet to pinch off by Rayleigh instability. In the electrospray regime where the electric field is larger than the Taylor cone formation threshold, the flow rate of the dispersed phase has to be small so that the produced droplets travel inside the channel without coalescense.

Using the AC electric field, the droplet size is changed as the voltage changes. The droplet size is dependent on the voltage as well as the balance of the emission flow rate from the tip and the supplied flow rate from the inlet. The tip position of the water is related to the droplet size. The lower tip position from the orifice generates the smaller droplets.

At some flow rates, the microfluidic device generates the bigger droplet followed by the smaller one successively. The simulation results show the velocity inside of the tip still moves downstream after it generates a big droplet. Therefore, the tip generates another smaller droplet while the tip is stretched. Then, the tip is retracted and commences a new cycle.

REFERENCES

1. G. M. Whitesides, “The origins and the future of microfluidics,” Nature **442**, 368, (2006).
2. S. L. Anna, N. Bontoux, and H. A. Stone, “Formation of dispersions using ‘flow focusing’ in microchannels,” Appl. Phys. Lett. **82**, 364 (2003).
3. S. L. Anna and H. C. Mayer, “Microscale tipstreaming in a microfluidic flow focusing device,” Appl. Phys. Lett. **18**, 121512 (2006).
4. J. B. Fenn, M. Mann, C. K. Meng, S.F. Wong, and C. M. Whitehouse**, “**Electrospray ionization for mass spectrometry of large biomolecules,” Science **246**, 4926 (1989).
5. A. G. Bailey, *Electrostatic Spraying of Liquids*, John Wiley & Sons, New York, (1988).
6. L. Rayleigh, “On the Equilibrium of Liquid Conducting Masses Charged with Electricity,” Phil. Mag. **14 Ser. 5**, 184-6 (1882).
7. J. Zeleny, “Instability of Electrified Liquid Surface,” Phys. Rev. **10**, 1, 1-6 (1917).
8. B. Vonnegut and R. L. Neubauer, “Production of Monodisperse Liquid Particles by Electrical Atomization,” J. Colloid Sci. **7**, 616 (1952).
9. G. I. Taylor, “Disintegration of Water Drops in an Electric Field,” Proc. Royal Soc. **A28** (1964).
10. M. Mutoh, S. Kaieda and K. Kamimura, “Convergence and Disintegration of Liquid Jets Induced by an Electrostatic Field,” J. Appl. Phys. **50**, 3174 (1979).

11. I. Hayati, A. I. Bailey and Th. F. Tadros, “Mechanism of stable jet formation in electrohydrodynamic atomization,” Nature **319**, 2 (1986).

12. M. Sato, T. Hatori and M. Saito, “Experimental Investigation of Droplet Formation Mechanisms by Electrostatic Dispersion in a Liquid-Liquid System,” IEEE Trans. Ind. Appl., **33,** 6 (1977).

13. A. Barrero, J. M. Lepez-Herrera, A. Boucard, I. G. Loscertales and M. Marquez, “Steady Cone-jet Electrosprays in Liquid Insulator Baths,” J. Colloid Interface Sci. **272**, 104-108 (2004).

14. P. Garstecki, H. A. Stone and G. M. Whitesides, “Mechanism for Flow-Rate Controlled Breakup in Confined Geometries: A Route to Monodisperse Emulsions,” Phys. Rev. Lett. **94**,164501 (2005).

15. M. A. Holden, S. Kumar, E. T. Castellana, A. Beskok and P. S. Cremer, “Generating fixed concentration arrays in a microfluidic device,” Sensors and Actuators B, **92** (2003).

16. J. C. McDonald, D. C. Duffy, J. R. Anderson, D. T. Chiu, H. Wu, O. J. A. Schueller, and G. M. Whitesides, “Fabrication of microfluidic systems in poly (dimethylsiloxane),” Electrophoresis **21**, 27 (2000).

17. L. Rayleigh and J. W. Strutt, “Investigation of the character of the equilibrium on an incompressible heavy fluid of variable density,” Proceedings of the London Mathematical Society, (1883), Vol. **14**, 170 - 177.

18. D. R. Link, E. Grasland-Mongrain, A. Duri, F. Sarrazin, Z. Cheng, G. Cristobal, M. Marquez, and D. A. Weitz, “Electric Control of Droplets in Microfluidic Devices,” Angew. Chem. Int. Ed. **45**, 2556 (2006).

19. M. R. Davidson, D. J. E. Harvie, and J. J. Cooper-White, “Flow focusing in microchannels,” ANZIAM J. **46E**,C47 (2005).

20. C. Zhou, P. Yue and J. J. Feng, “Formation of simple and compound drops in microfluidic devices,” Phys. Fluids **18**, 092105 (2006).

21. Z. Cheng, “Dynamics of drop production in hydrodynamic flow focusing microfluidic devices: periodic behaviors and chaos,” Proceedings of the 4th International Conference on Computing, Communications and Control Technologies, (2006), p. 155-160.

VITA

NAME:	Haejune Kim
PERMANENT ADDRESS:	247-6 Sawoo-dong Gimpo-si, Kyounggi-do. South Korea.
EDUCATIONAL BACKGROUND:	M.S. Mechanical Engineering, Texas A&M University, College Station, Texas, USA. August 2008.
	B.S. Mechanical Engineering, Korea University, Seoul, South Korea. March 2004.